11.5 A 2-Phase Soft-Charging Hybrid Boost Converter with Doubled-Switching Pulse Width and Shared Bootstrap Capacitor Achieving 93.5% Efficiency at a Conversion Ratio of 4.5

Mo Huang[1,2], Yan Lu[1], Rui P. Martins[1,3]

[1]University of Macau, Macau, China
[2]South China University of Technology, Guangzhou, China
[3]University of Lisboa, Lisbon, Portugal

High conversion ratio (CR) boost converters are in high demand for LED backlighting in a multitude of products including smartphones and tablets. The conventional boost (CB) converter with high CR has large inductor current ripples, thus requiring high-quality inductor to mitigate the efficiency degradation. Meanwhile, a narrow switching pulse width in the high CR converters limits the switching frequency (f_{SW}). The hybrid converter with flying capacitors (C_F) can widen the pulse width for the same CR, but hard-charging has been an issue in previous works [1-3].

Figure 11.5.1 shows the proposed 2-phase soft-charging hybrid boost (HB) converter, consisting of two branches. Each branch has an inductor L_1 (L_2), a flying capacitor C_{F1} (C_{F2}), and three switches M_1 (M_2), M_3 (M_4), M_5 (M_6). It operates in three states. In state-1, M_1, M_3, M_5 are on while M_2, M_4, M_6 are off. L_1 is energized, and current of L_2 (I_{L2}) decreases with a slope of α, and is divided into two parts, I_{C1} that flows into C_{F1} and I_{C2} that flows into the output (C_{F2} in series with output capacitor C_O). Considering $C_O \gg C_{F2}$, I_{C1} and I_{C2} are almost equal but they have opposite polarities, hence, both have a slope of $\alpha/2$. The status reverses in state-2. In state-3, M_1 and M_2 turn on while others turn off, hence, L_1 and L_2 are charged and there would be no change on C_{F1} and C_{F2}. The proposed HB works with state-1→state-3→state-2→state-3 periodically.

There are several benefits for this scheme. 1) The 2-phase operation reduces input and output ripples. 2) Since there is no direct charge transfer between C_{F1} and C_{F2}, nor between C_F and C_O, soft-charging is achieved. 3) Only M_3 and M_4 need to sustain a high V_{DS} that is V_O in state-2 and state-1, whereas other switches can use lower voltage devices as their V_{DS} stresses are only $V_O/2$, reducing the switching losses and silicon area. 4) Due to C_{F1} and C_{F2} charge balancing, V_{C1} and V_{C2} should be $V_O/2$, and $CR=2/(1-D)$, where D is the duty cycle. Here, for the 2-phase operation, D should be larger than 0.5, and thus the minimum CR is four. Comparing to the conventional boost, we double the switching pulse-width for the same CR, allowing a higher f_{SW}.

Figure 11.5.2 presents the schematic of the proposed HB. We use NMOS switches to reduce the silicon area and gate capacitances. A separate gate-drive voltage V_{DR}=5.5V is used for low conduction losses. M_3 and M_4 are isolated devices with a V_{DS} rating of 20V, while others use 10V devices. Due to the floating sources of M_{3-6}, their gate-drive supplies V_{DR34}, V_{DR5}, V_{DR6} should be bootstrapped. A type-III compensation network is used, in which the error between V_O and V_{REF} is filtered and then compared with a saw-tooth wave working at $2 \times f_{SW}$. The following 2-phase generator divides the compared output by two, and reconstructs it into the PWM control signals for each phase at f_{SW}.

Figure 11.5.3 illustrates the schematic of the bootstrap generator and the gate-drive scheme. The deadtime DT_1 is added between the control signals S_1 and S_4 (S_2 and S_3), to prevent the feedthrough from V_3 (V_4) to the ground. For the bootstrap capacitors of M_3 and M_4, they should be several times larger than the gate capacitance. For a 2-phase CB (2P-CB), two bootstrap capacitors may be required for independent gate-drive supplies, doubling the area. However, considering that M_3 and M_4 only turn on alternatively in the proposed HB, the bootstrap capacitor (C_{34}) can be shared without doubling the area. C_{34} can drive M_3 and M_4 in state-1 (at t_1) and state-2 (at t_3), respectively, and be charged by V_{DR} in state-3 (at t_2 and t_4), through an active diode D_{34} controlled by S_A. The interleaved charging of M_3 and M_4 is obtained by connecting the bottom plate of C_{34} to either V_1 or V_2 through the switches M_B or M_C. Another deadtime, namely, DT_2 is added between S_B and S_C, to prevent V_1 and V_2 feedthrough. For the gate-drive supplies V_{DR5} and V_{DR6} of M_5 and M_6, they should be charged by a voltage source $V_O/2+V_{DR}$ first, then be bootstrapped to V_O+V_{DR} in state-1 or state-2. Coincidently, V_{DR34} is bootstrapped to $V_O/2+V_{DR}$ in both state-1 and state-2, and thus can be reused to charge the bootstrap capacitors C_5 and C_6. In state-1, C_6 is charged from V_{DR34} through an active diode D_6, while C_5 discharges to M_5 (at t_1),

and vice versa in state-2 (at t_3). As V_{DR34} is reused to charge C_5 and C_6, an additional drop on V_{DR34} will occur at t_1 and t_3. However, thanks to the proposed topology, M_5 and M_6 are relatively small since they have low voltage stress and small high-side (HS) currents (to be explained next). This reduces both the sizes of C_5 and C_6, and the V_{DR34} drop.

Figure 11.5.4 normalizes the power losses of the proposed HB to those of a 2P-CB, with CR=4.5. We choose both the same inductor DCR and switch on-resistance (R_{ON}) for the two topologies. However, all the switches in 2P-CB should use 20V devices. The calculated inductor DCR loss in the proposed design is lower than that of a 2P-CB, because the ripple of I_L decreases with a smaller inductor voltage swing. This relaxes the inductor DCR requirement, reducing the inductor volume and cost. Thus, in the proposed design, we use 3.3μH inductors in 3010 package with a DCR of 166mΩ, instead of a 4020 package with a DCR of 38mΩ. Although we use two HS switches M_3 (M_4) and M_5 (M_6) in each phase, the summed conduction loss is still lower since they only conduct half of I_L with a reduced current ripple. However, the conduction loss of the low-side (LS) switches M_1 and M_2 is thereby higher. Since the HS root-mean-square (RMS) current is much smaller than that of the LS, smaller HS switches can be used. For the switching losses, all the switches benefit from the halved V_{DS} swing, while the low-stress switches further enjoy a reduced gate charge (Q_G). Thus, the switching losses of M_1, M_2, M_5, M_6 are only 0.11 times, and M_3, M_4 are 0.56 times that of the 2P-CB. The gate loss of LS decreases to 0.26 times from the C_{GS} reduction of the low-stress device, while that of the HS slightly increases by 1.26 times as a sum of two switches.

Considering the mismatches on L_1 and L_2, the inductor currents can be automatically balanced, because the error from mismatch is fed-back through the C_{F1} and C_{F2}, ensuring the charge balancing ($Q_1=Q_2$) and removing the conventional phase currents balancing. For the mismatches on the C_{F1} and C_{F2}, I_{C1} and I_{C2} will be different, but the ΔV_{C1} and ΔV_{C2}, caused by I_C discharging from the respective C_F, will compensate each other and leave V_O unchanged. The mismatch effects on CR are also minor, as $R_L \times (C_{F1}+C_{F2})$ can be much larger than $1/f_{SW}$, where R_L is the load resistance.

Figure 11.5.7 shows the chip micrograph of the proposed HB that is fabricated in a 0.35μm HV CMOS process, where the core area occupies 1.15mm×0.75mm. M_1 and M_2 have a large size to accommodate a high RMS current. We use f_{SW}=2MHz to balance the conduction and switching losses with smaller passives. C_O=10μF and $C_{F1}=C_{F2}$=0.47μF, and their ESRs can also be relaxed because of the reduced HS RMS currents. Figure 11.5.5 plots the steady-state waveforms of V_1, V_2, I_{L1}, I_{L2}, and V_O, where V_{IN}=4V, CR=5, and I_O=100mA. A 20V V_O is obtained, with 15mV ripples. The measured peak efficiency is 93.5% at V_{IN}=4.2V, CR=4.5, and I_O=100mA, and is 91.7% at V_{IN}=3.3V, CR=6, and I_O=75mA. The efficiency drops when CR increases, due to the more conduction losses on M_1 and M_2. We estimate the power loss break-down, where the LS conduction loss is the largest portion as predicted. Figure 11.5.6 shows the performance comparison table. From the reduced voltage stress and shared M_3/M_4 bootstrap capacitor, we have achieved a small area. Also, we have reached higher efficiencies than the CB at high CRs, because of the reduced RMS currents, reduced switching losses, and the doubled pulse-widths. As compared to the previous HBs, this work prevents C_F hard charging, and thus it achieves higher efficiency with smaller C_F value. The efficiency can be improved by further optimizing transistor sizing, as in the current form the conduction loss dominates.

References:
[1] S. Shin et al., "A 95.2% Efficiency Dual-Path DC-DC Step-Up Converter with Continuous Output Current Delivery and Low Voltage Ripple," *ISSCC*, pp. 430-431, Feb. 2018.
[2] S. Marconi et al., "A Novel Integrated Step-Up Hybrid Converter with Wide Conversion Ratio," *IEEE Trans. Power Electron.*, early access, DOI: 10.1109/TPEL.2019.2931875, July 2019.
[3] C. Hardy and H. Le, "A 10.9W 93.4%-Efficient (27W 97%-Efficient) Flying-Inductor Hybrid DC-DC Converter Suitable for 1-Cell (2-Cell) Battery Charging Applications," *ISSCC*, pp. 150-151, Feb. 2019.
[4] Texas Instruments, "TPS61181A White-LED Driver for Notebook Display," Datasheet, Feb. 2011. Accessed on Nov. 29, 2019, <http://www.ti.com/lit/ds /symlink/tps61181a.pdf>.
[5] T. Kong et al., "A 0.791 mm^2 On-Chip Self-Aligned Comparator Controller for Boost DC-DC Converter Using Switching Noise Robust Charge-Pump," *IEEE JSSC*, vol. 49, no. 2, pp. 502-512, Feb. 2014.
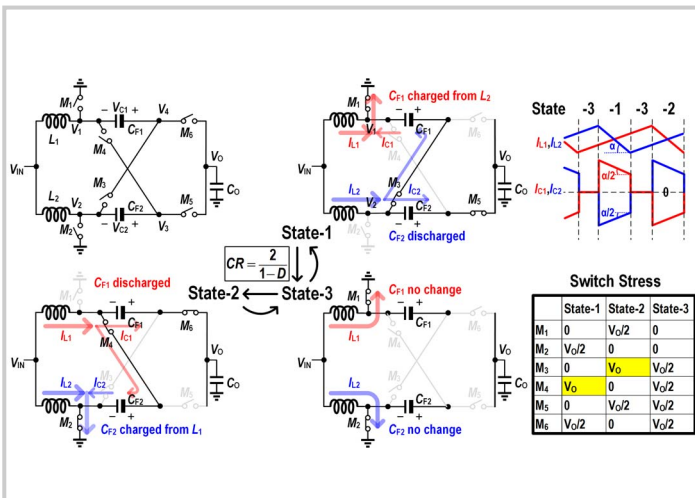
Figure 11.5.1: Topology and working principle of the proposed 2-phase HB (left), its current profiles (top right), and the V_{DS} stress of all the switches (bottom right).
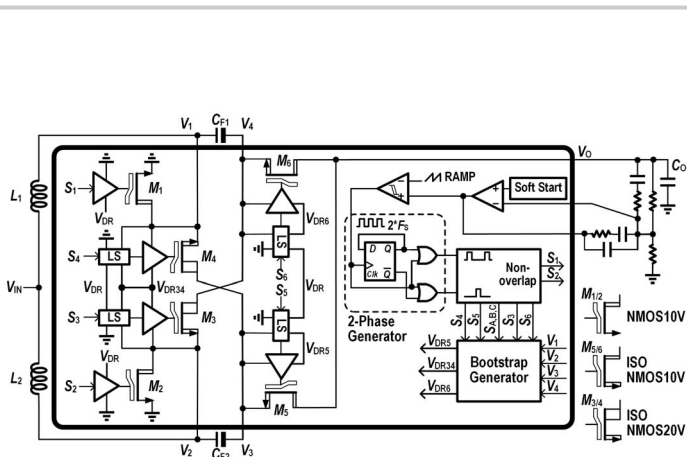

Figure 11.5.2: Schematic of the proposed 2-phase HB converter.
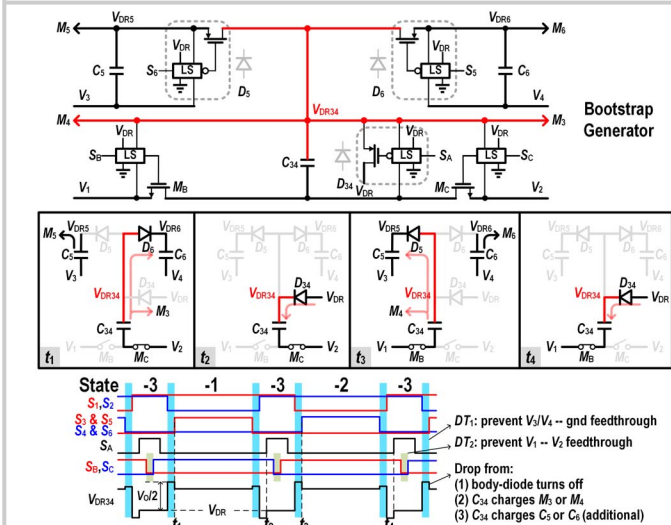
11

Figure 11.5.3: Schematic of the bootstrap generator (top), Working principles (middle), and timing diagram (bottom) of the bootstrap gate-drive scheme.
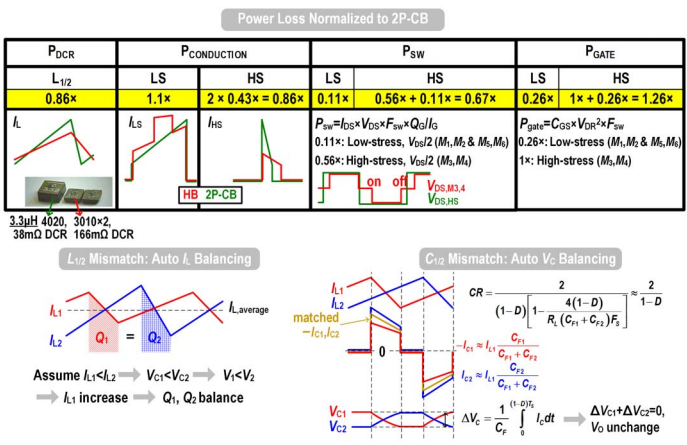

Figure 11.5.4: The power loss normalized to the 2P-CB (top) at CR=4.5. The auto I_L balancing with L_1 and L_2 mismatch (bottom left), and V_C balancing with C_{F1} and C_{F2} mismatch (bottom right).

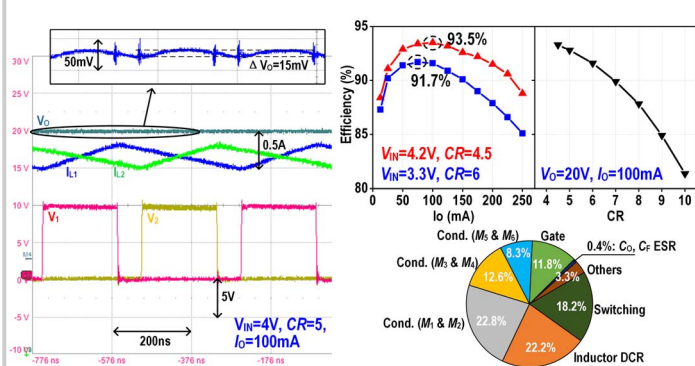**Figure 11.5.5:** Measured transient waveform of the proposed HB, when V_{IN}=4V, CR=5, I_0=100mA (left). Measured efficiencies versus I_0 and CR (top right). Calculated power loss breakdown when V_{IN}=4.2V, CR=4.5, I_0=100mA (bottom right).

	TI TPS61181A[4]	2014 JSSC [5]	2018 ISSCC [1]	2019 TPE [2]	This work
Process	n.a.	0.35um BCD	0.18um BCD	n.a.	0.35um CMOS
Area	n.a.	1.86mm²	6mm²	8mm²	0.86mm²
Topology	Conventional boost	Conventional boost	Hybrid boost	Hybrid boost	Hybrid boost
Input Voltage	4.5-27V	2.7-4.5V	2-4.2V	6-18V	2-4.4V
Output Voltage	4.5-38V	8V	3-5V	12-50V	9-20V
Load Current (I_L)	20-120mA	20-300mA	10-800mA	70-100mA	10-250mA
F_{SW}	1MHz	1MHz	1MHz	Max. 820kHz	2MHz
Multi-Phase	No	No	No	No	Yes
CR	$\frac{1}{1-D}$	$\frac{1}{1-D}$	$\frac{2-D}{2-2D}$	$\frac{3-D}{1-D}$	$\frac{2}{1-D}$
Inductor L (DCR)	10µH (53mΩ)	10µH (11mΩ)	4.7µH (200mΩ)	18µH (n.a.)	2×3.3µH (166mΩ)
Output Capacitor	4.7µF	10µF	10µF	10µF	10µF
Flying Capacitor	n.a.	n.a.	10µF	2×260µF	2×0.47µF
Soft Charging	n.a.	n.a.	No	No	Yes
Peak Efficiency @ (CR)	94% (CR=1.67)	90% (CR=2.16)	95.2% (CR=1.4)	92% (CR=2.5)	93.5% (CR=4.5)
Effieicncy @ CR=6 (I_L=)	87.9% (I_L=70mA)	n.a.	n.a.	88.2% (I_L=70mA)	91.7% (I_L=75mA)

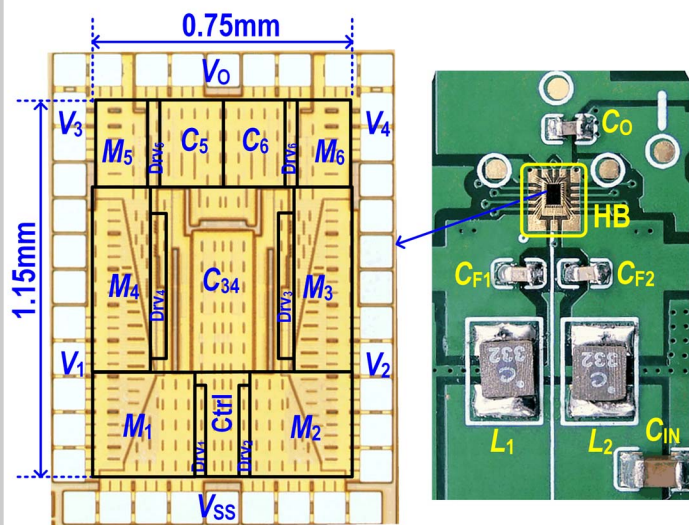**Figure 11.5.6:** Performance comparison with the state-of-the-art.

Figure 11.5.7: Chip micrograph and PCB of the proposed HB.